Dependence of contrail characteristics on the distribution law of parameters of nonisobaric exhaust jet at nozzle exit

A.V. Kashevarov, A.N. Kucherov, and G.V. Molleson

N.E. Zhukovskii Central Aerohydrodynamic Institute, Moscow

Received March 15, 2001

It is shown that the parameters of a contrail of a large civil aircraft (distance to the contrail and the time of its formation, contrail cross size, ice content, water content, cross optical thickness) depend strongly on the exhaust/atmosphere pressure ratio (parameter of jet nonisobarisity) and the distribution law of jet parameters at an exhaust nozzle of an aircraft engine. The initial part of the pressure leveling-off in the nonisobaric jet is described by full Navier–Stokes equations and calculated by the method of large particles. The far field, including the contrail, is described by the parabolized equations like Prandtl boundary layer equations and calculated by the finite-difference algorithm. The coefficients of radiation scattering and absorption by liquid water droplets and ice crystals are calculated using the Mie theory with allowance for the particle size distribution. It is shown that a clearing channel can be created by a laser pulse of relatively low power.

Introduction

The growing interest to the study of contrails is caused by the effect of aircraft engine emissions on the upper atmospheric layers and possible influence of aircraft on the climate.[1–8] A contrail is formed at a long distance from an aircraft exceeding the nozzle exit radius by an order of magnitude and even more. As a rule, axisymmetric isobaric exhaust jets with a homogeneous initial distribution of parameters in the nozzle cross section are considered.[5,8–10] It is assumed that disturbations in the initial section of the jet have no effect on the far field of temperature, velocity, concentration of exhaust gases and products of chemical reactions, as well as the contrail. In Ref. 11, this assumption was shown to be incorrect, at least, relative to phase transitions of the exhaust mixture.

Relatively small variations of the mean temperature at the nozzle exit can alter by 100% the distance to the contrail, its ice and water content, and optical thickness. The jet nonisobarisity gives rise to the system of spikes or the area with high gradients of gas-dynamic parameters, in which the pressure levels off at the atmospheric value. Different distribution laws of the parameters over the nozzle cross section can change the shape of the condensation (crystallization) surface in the far field of the jet. In Refs. 12 and 13 it was shown that the nonisobarisity could affect considerably the initial characteristics of the contrail.

The preliminary studies using, as an example, the model distribution laws of the parameters at the nozzle exit of the Boeing 747–400 aircraft showed their significant effect on the initial characteristics of the contrail (~100%). In some cases, the contrail may be formed in the distributed field of initial parameters, but it is not formed at all in the homogeneous field. Jets, equivalent in the mass consumption of mixture and vapor, as well as with the same total energy of gas were considered. In this paper, using the model distributions of the initial parameters of the jet at the nozzle exit, we study the effect of nonisobarisity and the distribution law on the contrail, as well as the effects of atmospheric conditions and the phase state (water–ice) of aerosol particles.

1. Calculation of nonisobaric part of the jet within the framework of the Navier–Stokes equations

For the Boeing 747–400 aircraft[9] in the cruising flight (height 10.6 km, pressure $p_\infty = 0.239$ bar, atmospheric temperature $T_\infty = 219$ K, speed $u_\infty = 237$ m/s): in the hot core on the axis $0 < r < r_a/2$ the exhaust temperature is $T_0 = 590$ K, the mole fraction of vapor is $C_{H_2O} = 0.0428$ (vapor density $\rho_{v0} = 0.00375$ kg/m^3), and mixture speed is $u_0 = 437$ m/s. The nozzle radius is $r_a = 1.1$ m, the relative atmospheric humidity is $S_\infty = 0–0.71$ ($\rho_{v\infty} = 0–4.80 \cdot 10^{-5}$ kg/m^3). At the distance $r = r_a$ from the axis, the temperature and speed are $T_1 = 284$ K and $u_1 = 316$ m/s. Let the vapor density at this distance be $\rho_{v1}|_{r_a} = 0.4\rho_{v0} \approx 0.00150$ kg/m^3. Let distributed parameters at the nozzle exit be described by the following equations:

Version I:

at $0 \le r \le r_a/2$

$$u = u_0;\ T = T_0;\ \rho_v = \rho_{v0} = 0.00375 \text{ kg/m}^3;$$

at $r \ge r_a/2$

$$u(r) = u_\infty + a_1 e^{-(r/r_a)^2} + a_2 e^{-(1-2r/r_a)^2} + a_3 e^{-(1-r/r_a)^2},$$

0235-6880/01/05 377-06 $02.00

$$T(r) = T_\infty + b_1 e^{-(r/r_a)^2} + b_2 e^{-(1-2r/r_a)^2} + b_3 e^{-(1-r/r_a)^2},$$

if $T < T_\infty$, then $T = T_\infty$,

$$\rho_v(r) = \rho_{v\infty} + c_1 e^{-(r/r_a)^2} + c_2 e^{-(1-2r/r_a)^2} + c_3 e^{-(1-r/r_a)^2},$$

$$a_3 = a_1, \quad a_2 = u_0 - u_\infty - 2a_1 e^{-1/4}, \qquad (1)$$

$$a_1 = \frac{u_\infty(1 - e^1) - u_0 + u_1 e^1}{1 + e^1 - 2e^{-1/4}}.$$

In the coefficients b and c, u_∞, u_0, and u_1 should be replaced by T_∞, T_0, T_1 and $\rho_{v\infty}$, ρ_{v0}, ρ_{v1}, respectively.

Version II. The parameter values equivalent and homogeneous over the nozzle exit are calculated from the laws of conservation of the mass of the mixture and vapor, as well as the energy of the gas mixture

$$\pi r_a^2 \rho_a u_a = C_1 = \int_0^{r_a} 2\pi r \rho(r) u(r) dr, \quad \rho(r) = p\mu/RT(r),$$

$$\pi r_a^2 \rho_a u_a (C_p T_a + u_a^2/2) = C_2 =$$

$$= \int_0^{r_a} 2\pi r \rho(r) u(r) [C_p T(r) + u^2(r)/2] dr,$$

$$\rho_a = \frac{C_1}{\pi r_a^2 u_a}, \quad T_a = \frac{p_\infty \mu}{R\rho_a},$$

$$u_a = \frac{-B + \sqrt{B^2 + 2C_1 C_2}}{C_1}, \quad B = \frac{\pi r_a^2 C_p p_\infty \mu}{R}$$

$$\pi r_a^2 \rho_{v\,a} u_a = C_3 = \int_0^{r_a} 2\pi r \rho_v(r) u(r) dr, \quad \rho_{v\,a} = \frac{C_3}{\pi r_a^2 u_a}. \qquad (2)$$

At $p_a = p_\infty$ we have $T_a = 465.2$ K, $u_a = 396.4$ m/s, $\rho_a = 0.179$ kg/m^3, $\rho_{va} = 0.00306$ kg/m^3.

In the version IIa, the air temperature is $T_\infty = 224$ K, and all other parameters are unchanged. In versions III and IV, we consider the nonisobaric jet at $N = p_{aN}/p_\infty = 1.2$ with the distributed parameters $u(r)$, $T(r)$, $\rho_v(r)$ (III) and parameters u_{aN}, T_{aN}, $\rho_{v,aN}$ homogeneous across the nozzle (IV).

In the version IV, homogeneous values of the gas-dynamic parameters are calculated under the condition that the Mach number is constant $M_a = M_{aN} = \text{const}$ in the cruising flight. This condition can be fulfilled by changing the fuel Δq_f and energy $E_f \Delta q_f$ consumption

$$\rho_a u_a (1 + \varepsilon) = \rho_{aN} u_{aN}, \quad \rho_a u_a (H_a + \varepsilon E_f) = \rho_{aN} u_{aN} H_{aN},$$

$$\rho_{v\,a} u_a + \varepsilon \rho_a u_a E_w = \rho_{v\,aN} u_{aN}; \quad \frac{u_a}{\sqrt{T_a}} = \frac{u_{aN}}{\sqrt{T_{aN}}},$$

$$N = \frac{\rho_{aN} T_{aN}}{\rho_a T_a},$$

$$\varepsilon = \frac{\Delta q_f}{\rho_a u_a} = \left(\frac{1}{2} + \frac{H_a}{2E_f}\right)\left[\sqrt{1 + \frac{4(N^2-1)H_a/E_f}{(1 + H_a/E_f)^2}} - 1\right],$$

$$u_{aN} = \frac{N}{1+\varepsilon} u_a, \quad T_{aN} = \left(\frac{N}{1+\varepsilon}\right)^2 T_a, \quad Y_{aN} = \frac{Y_a + \varepsilon E_w}{1+\varepsilon}, \qquad (3)$$

where E_f (≈ 43 MJ/kg kerosene) is the fuel heating value; E_w (≈ 1.25 kg/kg fuel) is the water emission index; $H = C_p T + u^2/2$ is the enthalpy of the mixture. At $M_a = 0.917$ and $N = 1.2$ we have $T_{aN} = 662.7$ K, $u_{aN} = 473.1$ m/s, $\rho_{aN} = 0.151$ kg/m^3, $\rho_{v,aN} = 0.00358$ kg/m^3 ($\varepsilon = 0.00543$).

For *version III*, the distributions of the parameters over the nozzle exit (at $0 \le r \le r_a$) are taken to be proportional to the laws of the version I [see Eq. (1)]:

$$u_N(r) = u(r)\frac{u_{aN}}{u_a}, \quad T_N(r) = T(r)\frac{T_{aN}}{T_a}, \quad \rho_{vN}(r) = \rho_v(r)\frac{\rho_{vaN}}{\rho_{va}},$$

and if $r > r_a$, $u_N(r) = u(r)$,

$$T_N(r) = T(r), \quad \rho_{vN}(r) = \rho_v(r). \qquad (4)$$

The origin of coordinates is at the center of the nozzle exit section. The Navier–Stokes equations[14] for the axisymmetric jet were calculated in the area $2 \le x/r_a \le 12$ and $0 \le r/r_a \le 3$. The boundary conditions are the parameters of the approach flow and the parameters of the environment at the boundary of the calculation domain. In solution was used the method of large particles.[15]

Figure 1 shows the temperature distributions along the axis and across the jet. Excess pressure in the versions III and IV accelerates the flow, and viscosity smoothes out the cross profiles. The pressure levels off at the atmospheric value with the distance $x \approx 3$–$4\ r_a$. The temperature decreases to the pressure leveling-off cross section, the speed increases, and the concentration of vapor and chemically neutral gases does not change.

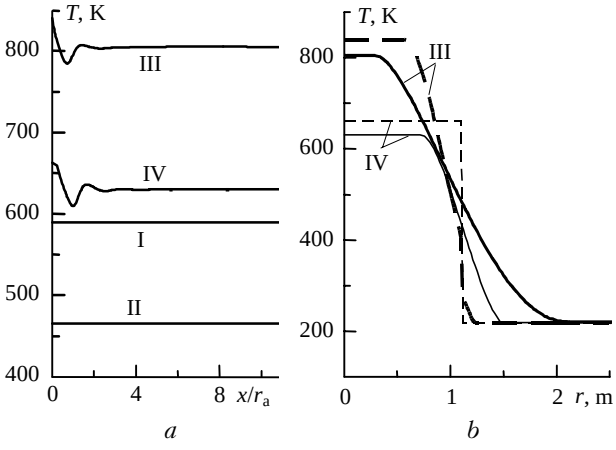

Fig. 1. Temperature distribution: along the axis, versions I–IV (*a*); across the jet, versions III–IV, at the nozzle exit section of the radius $r_a = 1.1$ m (dashed curves) and at the distance $x/r_a = 12$ (solid curves) (*b*).

2. Calculation of turbulent diffusion of the jet within the framework of Prandtl equations

The formulation of the problem is given in Ref. 16. The turbulent Prandtl and Schmidt numbers were taken equal to unity: $\mathrm{Pr_T} = C_p\,\mu_T/\lambda_T = 1 = \mathrm{Sc_T} = \mu_T/\rho D_T$. Here μ_T, λ_T, and D_T are the coefficients of turbulent viscosity, thermal conductivity, and diffusion. Two-parameter k–e model of turbulence was used, for which the distributions of the specific (per unit mass) turbulence energy $k_T = V_T^2/2$ (V_T are turbulent pulsations of velocity) and dissipation rate of turbulent pulsations in the jet $e_T = 0.09\rho k_T^2/\mu_T$ are described by the well-known parabolic-type equations.[17]

In the initial cross section, we took $\nu_{T\infty} = \mu_{T\infty}/\rho_\infty = 0.225$ m^2/s, $k_{T\infty} = 1.125$ m^2/s^2 in the external flow, $\nu_{T0} = 0.01\,\nu_{T\infty}$, $k_{T0} = (0.01\,u_a)^2/2$ inside the nozzle; $\nu_{Ta} = 100\,\nu_{T\infty}$, $k_{Ta} = 2\cdot10^4$ m^2/s^2 on the nozzle edge. The parameter n is the number concentration of droplets (and condensation nuclei – soot particles) was taken equal to 10^{13} in the case of the homogeneous distribution and proportional to the relative distribution law (1) across the nozzle in the rest of cases.

For the nonisobaric jet, the initial conditions were set as the solutions of the Navier–Stokes equations in the cross section $x = 12r_a$. Droplets (particles) were assumed to be "frozen" into the gas. The droplet radius was determined as $a = (3\rho Y_{w,i}/4\pi n\rho_{w,i})^{1/3}$, where $\rho_{w,i} = 10^3$, 900 kg/m^3, $Y_{w,i} = \rho_{w,i}/\rho$ are the density and relative mass concentration of water and ice; $\rho_{w,i}$ and ρ are the water (ice) content and aerosol density. Coagulation of particles at collisions was taken into account.

All the sought parameters almost do not change at the initial part of the turbulent jet,[18] then they sharply decrease inversely proportional to some degree of the distance from the nozzle, and near the condensation cross section they are slightly decreasing functions.

3. Initial characteristics of the contrail

The contrail in the near zone has the form of a tube with the walls thickening gradually until complete filling the tube with aerosol. The calculations were performed from the nozzle exit ($x = 0$) to the cross section of aerosol closure on the jet axis $x = x_*$ and further up to the cross section $x = 1000$ m for the versions I–IV.

The distributions of the water and ice content functions along the jet axis for the versions I and II at different relative atmospheric humidity, as well as the cross distributions of the ice content function at the aerosol closure cross section are shown in Fig. 2. Figure 3 shows the radii of the particles $a(x,\ r = 0)$ along the jet axis (a) and across the jet $a(x = x_*,\ r)$ (b) in the cross section of aerosol closure on the axis $x = x_*$. Table 1 gives the values of the coordinate x_* for the versions I, II, III, IV, cross dimensions of contrails r_c in the cross section $x = x_*$, the values of the maximum water and ice content $\rho_{w,i}(x_m) = \max[\rho_{w,i}(x,\ r = 0)]$, and the coordinates of this cross section $x = x_m$.

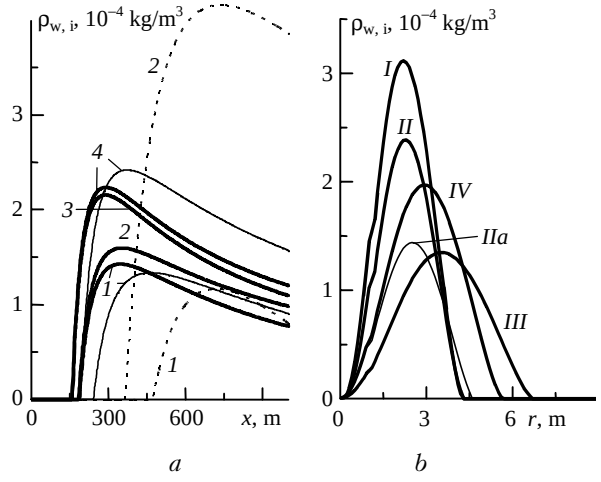

Fig. 2. Water (*1*, *2*) and ice (*3*, *4*) content functions of aerosol: along the jet axis (*a*) for the version I (bold solid curves), II (solid curves), and II*a* (dashed curves) at the relative atmospheric humidity $S_\infty = 0$ (*1*, *3*) and 0.71 (*2*, *4*); across the jet (*b*) for the versions I, II, II*a*, III, IV in the cross sections of closure of crystalline aerosol on the axis $x = x_* = 158.2$ (I), 191.2 (II), 354.9 (III), and 244.8 m (IV) at $S_\infty = 0.71$ for all the versions.

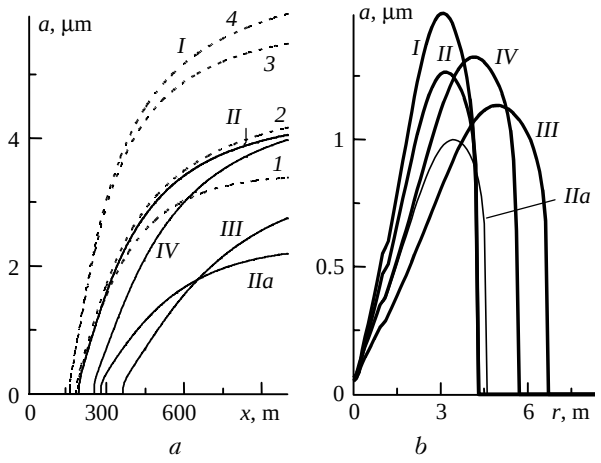

Fig. 3. Dependence of particle radii on the distance x along the axis from the nozzle exit (*a*): $a(x, 0)$: version I, water *1*, *2* and ice *3*, *4*, relative atmospheric humidity $S_\infty = 0$ (*1*, *3*) and 0.71 (*2*, *4*) (dashed curves); versions II, II*a*, III, IV, ice, $S_\infty = 0$ (solid curves); and on the distance r from the axis $a(x_*, r)$ in the cross section of closure of crystalline (ice) aerosol (*b*) on the axis $x_* \approx 158$, 191, 265.2, 355, and 244.8 m at $S_\infty = 0.71$ (versions I, II, II*a*, III, IV).

Table 1

Aerosol	Version							
	I		II		III		IV	
	S_∞							
	0	0.71	0	0.71	0	0.71	0	0.71
Distances x_*, in m, of beginning of condensation (water) and crystallization (ice) of aerosol								
water	186.5	183.2	241.7	231.4	528.3	474.8	329.4	303.4
ice	159	158.2	193.7	191.2	362.2	354.9	251.4	244.8
Contrail radius r_c, in m, at $x = x_*$								
water	4.12	4.37	4.18	4.47	6.28	7.10	5.45	5.89
ice	4.09	4.24	4.10	4.27	6.30	6.70	5.38	5.63
Maximum water/ice content $\rho_{w,i}(x_m)$, in 10^{-4} kg/m^3, and coordinate $x = x_m$, in m, (lower rows)								
water	2.015	2.252	1.333	1.640	0.466	0.770	0.933	1.307
	346	352	464	470	950	972	629	624
ice	3.043	3.157	2.261	2.416	1.218	1.369	1.787	2.000
	289	291	371	372	701	707	486	483

4. Optical thickness of the contrail

In the experimental study of contrails, an important role is played by the optical thickness

$$\tau(x) = \int_0^{r_c} \beta(\lambda, a, m)\rho_{w,i}(r)\mathrm{d}r, \qquad (5)$$

where $\beta(\lambda, a, m)$ is the specific (per unit mass) extinction coefficient at the wavelength λ in the polydisperse aerosol with the particle modal radius a and the parameter m of the particle size distribution. Because the elementary volume of the calculation domain on the scale of the jet cross dimension contains a large number of particles, the calculated radius a was taken as the modal radius (most probable). Reference 19 (p. 2797) gives the absorption coefficients for particles of different shape (spheres, needles (cylinders), disks (plates)). References 20 (Fig. 1) and 21 (Fig. 7) present the particle size dependences of the absorption and scattering coefficients, as well as the extinction coefficient $\beta(a)/\beta_{w,i}$ at $\lambda = 10.6$ μm for monodisperse and polydisperse (spheres, $m = 2$, the Khrgian–Mazin distribution[22]) water-droplet and ice aerosols (complex refractive indices are $m_{w,i} = n_{w,i} + i\kappa_{w,i} = 1.185 + i0.0690$ and $1.195 + i0.0602$; $\beta_{w,i} = 4\pi\kappa_{w,i}/\rho_{w,i}\lambda \approx 83.80$ m^2/kg are specific absorption coefficients in water and ice, respectively[23]). The calculations were made by the well-known equations of the Mie theory.[24] The extinction coefficients peak near $a \approx 2.65$ and 2.8 μm in the polydisperse aerosol and in the range of 9–10 μm in the monodisperse aerosol. Table 2 gives the maximum values of the optical thickness $\tau(x_\tau) = \max[\tau(x)]$ and the corresponding coordinates x_τ for the versions I, II, III, IV.

Figure 4 shows the dependence of the optical thickness $\tau(x)$ on the cross coordinate x under different conditions. The maximum of the optical thickness decreases 2.6 (curve *4*) – 3.2 (curve *1*) times due to the transition from the distributed parameters (version I) to the parameters constant across the nozzle (II). Then we compare the versions I–III and II–IV to separate the influence of nonisobarisity, the versions I–II and III–IV to demonstrate the effect of the distribution law, and the versions I–IV and II–III to analyze the joint effect of nonisobarisity and the initial distribution on the contrail parameters.

Table 2. Maximum cross optical thickness $\tau_{max} = \tau(x_\tau)$ of water-droplet/crystalline aerosol. The lower row gives the corresponding coordinate x_τ, in m

Aerosol	Version							
	I		II		III		IV	
	S_∞							
	0	0.71	0	0.71	0	0.71	0	0.71
water, τ_{max}	0.203	0.249	0.0625	0.0905	0.0524	0.128	0.0565	0.0985
x_τ	371	391	516	555	950	1000	683	717
ice, τ_{max}	0.351	0.375	0.130	0.146	0.215	0.265	0.139	0.164
x_τ	294	295	404	412	793	805	521	508

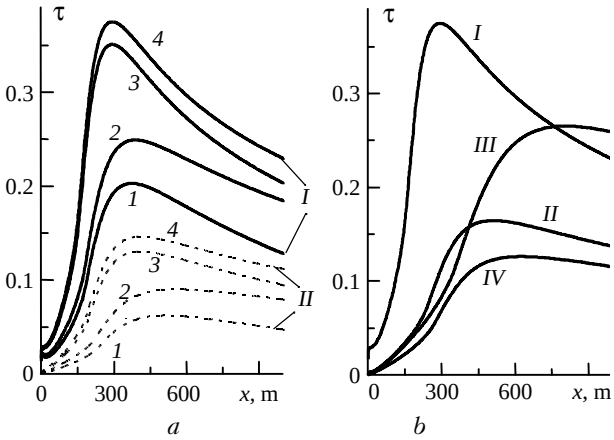

Fig. 4. Cross optical thickness of the contrail: (*a*) version I (solid curves), II (dashed curves), droplets at $S_\infty = 0$ (*1*), droplets at $S_\infty = 0.71$ (*2*), ice crystals at $S_\infty = 0$ (*3*), and ice crystals at $S_\infty = 0.71$ (*4*); (*b*) versions I, II, III, IV, ice, $S_\infty = 0.71$.

5. Influence of nonisobarisity

Consider now Tables 1 and 2. When passing from the version I with the parameters distributed over the nozzle exit to the version III with $N = p_{aN}/p_\infty = 1.2$, the distance x_* increases by 184, 159, 128, and 124% in the following situations: (1) water-droplet aerosol ($S_\infty = 0$); (2) water–droplet aerosol (0.71); (3) crystalline aerosol (0); (4) crystalline aerosol (0.71). The maximum cross optical thickness $\tau_{max} = \tau(x = x_\tau)$ decreases down to 26, 51, 61, and 71%. The cross dimension of the contrail r_c in the cross sections $x = x_*$ increases 1.52, 1.62, 1.54, and 1.58 times. Such differences can be observed experimentally.

When passing from the version II with the parameters constant over the nozzle exit section (under the condition that the total energy flux is equal to energy consumption) to the nonisobaric version IV, the contrail parameters change as follows: x_* increases 1.36, 1.31, 1.3, and 1.28 times; the value of τ_{max} changes by −10; +9, +7, and +12%; the radius r_c increases 1.3, 1.32, 1.31, and 1.32 times for the situations 1, 2, 3, and 4.

The temperature $T(0, x_*)$ on the axis in the aerosol closure cross section is: 248, 248.4, 252.2, 252.3 K (version I) and 236.6, 240.3, 245.1, 245.6 K (III), $\Delta T = T_I - T_{III} = 11.4 - 6.7$ K; 244.9, 245.8, 249.8, 250.1 K (II) and 239.1, 241.2, 245.5, 246.3 K (IV), $\Delta T = T_{II} - T_{IV} = 5.8 - 3.8$ K. When passing from the isobaric jet ($u = 260 - 264$ m/s; $N = 1$; version I) to the nonisobaric one ($u = 248 - 253$ m/s; $N = 1.2$; version III) the speed of the mixture in the cross sections $x = x_*$ decreases by 4 and 12 m/s in the case of the constant (II–IV) and distributed (I–III) parameters. The increase of the contrail cross dimension r_c in the cross sections $x = x_*$ in this case is illustrated by Figs. 2*b* and 3*b*. Note also that the particle size decreases (Fig. 3) and the condensate concentration decreases as well (Fig. 2). Thus, nonisobarisity with the excess pressure of 20% above the atmospheric value leads to the marked increase of the cross dimension r_c and the distance x_*, to the decrease of the water (ice) content, and to the change of the contrail optical thickness.

6. Jet inhomogeneity in the cross direction

In the isobaric jet ($N = 1$), when passing from the version I with the distributed parameters to the version II with the parameters constant across the nozzle exit, the distance to the contrail x_* increases 1.3, 1.26, 1.22, and 1.21 times in the following situations: (1) water-droplet aerosol ($S_\infty = 0$), (2) water-droplet aerosol (0.71), (3) crystalline aerosol (0), (4) crystalline aerosol (0.71). The maximum optical thickness τ_{max} decreases 3.25, 2.75, 2.7, and 2.57 times. The cross dimension of the contrail r_c in the cross section x_* changes by the value less than 2%.

In the nonisobaric jet with the pressure exceeding 1.2 times the atmospheric value, when passing from the distributed parameters (version III) to the constant ones (version IV), the distance x_* decreases 1.60, 1.56, 1.44, and 1.45 times in the situations 1, 2, 3, and 4. The optical thickness τ_{max} changes by +8, −23, −35, and −38%. The contrail radius r_c in the cross section $x = x_*$ decreases 1.15, 1.21, 1.17, and 1.19 times.

The optical thickness (I → II) and the distance x_* (III → IV) vary most markedly. The cross dimension varies only slightly.

7. Phase state and conditions in the atmosphere

The change of the relative humidity has a marked effect on the distance x_* for the contrails of crystalline aerosol. As the relative humidity of the atmosphere changes within the considered range $S_\infty = 0–0.71$, the changes of the maximum optical thickness achieve 23 and 144% in the case of crystalline and water-droplet aerosol (version III). Naturally, these situations are extreme; aerosol can contain simultaneously both the liquid and solid phases in various proportions. The changes of the cross dimension of the crystalline contrail when passing from the dry atmosphere to the humid one with $S_\infty = 0.71$ do not exceed 6%, and only in the case of the water-droplet aerosol (version III) they achieve 14%.

The effect of the atmosphere also includes the change of the phase state (liquid water – ice crystals), because it is caused, in the first turn, by the temperature T_∞. The differences due to the phase state can be as large as 46% for x_* and up to 6% at the radius r_c. The differences for τ_{max} are even larger: 1.73 times (for the version I), 2.08 times (II), 4.1 times (III), and 2.46 times (IV). In the case of the absolutely dry atmosphere, the differences are larger than at $S_\infty = 0.71$ (see Fig. 4*a*).

In the version II*a* with higher atmospheric temperature $T_\infty = 224$ K, the considerable changes of the contrail parameters as compared to the case $T_\infty = 219$ K (version I–IV) were found as well. The parameter x_* changes almost twice; the water and ice contents vary significantly too.

8. Joint effect of nonisobarisity and initial distributions

When passing from the isobaric jet with the parameters distributed across the nozzle exit (version I) to the nonisobaric jet with the parameters constant in the cross direction (IV), the following changes were found. The distance x_* increases 1.77, 1.66, 1.58, and 1.55 times in the situations 1–4; the maximum optical thickness τ_{max} decreases 3.6, 2.53, 2.52, and 1.42 times; the cross dimension (radius) r_c of the contrail increases 1.32, 1.35, 1.32, and 1.33 times.

When passing from the isobaric jet with the parameters constant in the cross direction (version II) to the nonisobaric jet with the parameters distributed in the cross direction (III), we obtain the following: the distance x_* increases 2.19, 2.05, 1.87, and 1.86 times; the maximum optical thickness τ_{max} changes by −16.4, +41, +65, and +82%; the cross dimension of the contrail r_c increases 1.5, 1.59, 1.54, and 1.57 times.

Comparing these results with the similar results of Sections 5 and 6, we come to the conclusion that two

factors exert the same effect on the initial characteristics of the contrail as each of them does individually.

In the considered examples, the optical thickness $\tau < 0.38$. Following Refs. 20 and 25, we arrive at the conclusion that a laser pulse with the duration ~10^{-3} s and intensity $\leq 10^7$ W/m^2 is capable of creating the clearing channel in the contrail for monitoring of pollutants on its axis.[8]

Conclusion

Nonisobarisity with the excess pressure of 20% above the atmospheric value leads to the increase of the cross dimension (1.5–1.6 times) and the distance x_* (2.2–2.8 times), to the decrease of the water/ice content (2.5–4 times) and the optical thickness (1.4–3.9 times) of the contrail at the distributions I, III of the initial parameters of the jet across the nozzle exit. If the parameters are homogeneous across the nozzle exit (II $\rightarrow$ IV), the changes of the optical characteristics of the contrail are somewhat smaller, but still considerable.

When passing from the distributed initial parameters at the nozzle exit to the equivalent homogeneous parameters, the optical thickness τ_{max} and the distance x_* change most markedly (2.6–3.3 times and 1.6–1.8 times, respectively). The cross dimension varies only slightly (by 5–20%).

As the relative atmospheric humidity S_∞ changes from 0 to 0.71, the differences in τ_{max} are up to 23% and 144% in the crystalline and water-droplet aerosol, version III. The difference in τ_{max} due to the change of the phase state (water–ice) can achieve 51–310%.

As the temperature T_∞ increases by 5°C, the water and ice content change significantly in the cross section x_* of aerosol closure on the axis. The distance x_* changes 1.4–2 times. The joint effect of the two factors on the contrail is the same as for each factor separately. A laser pulse of relatively low power is capable of creating the clearing channel in the cross section of the maximum optical thickness.

Acknowledgments

This work was partially supported by the Russian Foundation for Basic Research (Initiative Project "a" No. 99–01–00446 and Leading Scientific Schools No. 00–15–96069).

References

1. U. Schumann, Ann. Geophys. **12**, Nos. 10/11, 365–384 (1994).
2. "*1995 Scientific Assessment of the Atmospheric Effects of Stratospheric Aircraft*," Assessment Chair: R.S. Stolarski, NASA Reference Publication **1381** (Washington, 1995).
3. *Proceedings of International Colloquium on Impact of Aircraft Emissions upon the Atmosphere* (Paris, 1996), Vol. 1, pp. 1–378; Vol. 2, pp. 379–667.
4. U. Schumann, ed., *Pollutants from Air Traffic (Results of Atmospheric Research in 1992–1997 Years)* (German Aerospace Center, Oberpfafenhofen, 1997), 290 pp.
5. P. Fabian and B. Kärcher, Physics and Chemistry of the Earth **22 (6)**, 1–96 (1997).
6. O.B. Popovicheva, A.M. Starik, and O.N. Favorskii, Izv. Ros. Akad. Nauk, Ser. Fiz. Atmos. Okeana **36**, No. 2, 163–176 (2000).
7. I.L. Karol', A.A. Kiselev, Yu.E. Ozolin, and E.V. Rozanov, Izv. Ros. Akad. Nauk, Ser. Fiz. Atmos. Okeana **36**, No. 3, 339–348 (2000).
8. A.N. Kucherov, Atmos. Oceanic Opt. **13**, No. 5, 484–491 (2000).
9. B. Kärcher, J. Geophys. Res. D9 **100**, No. 9, 18835–18844 (1995).
10. B. Kärcher, Th. Peter, U.M. Biermann, and U. Sehumann, J. Atmos. Sci. **53**, No. 21, 3066–3083 (1996).
11. A.N. Kucherov, A.P. Markelov, A.A. Semenov, and A.V. Shustov, in: *Proc. of 5th Intern. Symp. on Aviation Technologies of XXI Century* (Zhukovskii, 1999), pp. 382–389.
12. A.N. Kucherov and G.V. Molleson, Inzh.-Fiz. Zh. **74**, No. 5 (2001).
13. A.N. Kucherov, in: *SOQUE Proceedings of International Conference LASERS'2000*, 4–8 December 2000, Albuquerque, New Mexico, USA, ed. by V.J. and T.A. Corcoran (STS Press, 2001), V. 23 (accepted for printing).
14. L.G. Loitsyanskii, *Fluid and Gas Mechanics* (Nauka, Moscow, 1987), 840 pp.
15. O.M. Belotserkovskii and Yu.D. Davydov, *Method of Large Particles in Gas Dynamics* (Nauka, Moscow, 1982), 391 pp.
16. A.V. Kashevarov, M.N. Kogan, A.N. Kucherov, and A.L. Stasenko, Atmos. Oceanic Opt. **10**, No. 12, 984–990 (1997).
17. V.S. Avduevskii, D.A. Ashratov, A.V. Ivanov, and U.G. Pirumov, *Supersonic Nonisobaric Gas Jets* (Mashinostroenie, Moscow, 1985), 248 pp.
18. G.N. Abramovich, *Applied Gas Dynamics*, (Nauka, Moscow, 1991), Part. 1, 600 pp.
19. A.N. Kucherov, Int. J. Heat and Mass Transfer **43**, No. 16, 2793–2806 (2000).
20. A.N. Kucherov, *Proceedings of SOQUE Int. Conf. LASERS'99 13–17* December, 1999, Quebec, Canada, ed. by V.J. and T.A. Corcoran (STS Press, 2000), Vol. 22, pp. 143–150.
21. A.V. Kashevarov, A.N. Kucherov, and G.V. Molleson, "*Comparison of the effect of nonisobarisity and the distribution laws at nozzle exit on the initial characteristics of contrail*," Preprint No. 128, N.E. Zhukovskii Central Aerohydrodynamic Institute, Moscow (2000), 24 pp.
22. I.P. Mazin and A.Kh. Khrgian, eds., *Clouds and Cloudy Atmosphere. Handbook* (Gidrometeoizdat, Leningrad, 1989), 647 pp.
23. W.W. Irvine and J.B. Pollack, Icarus **8**, No. 2, 324–360 (1968).
24. C.F. Bohren and D.R. Huffman, *Absorption and Scattering of Light by Small Particles* (Wiley, New York, 1983).
25. A.N. Kucherov, Atmos. Oceanic Opt. **7**, No. 10, 749–752 (1994); A.N. Kucherov, Kvant. Elektron. **22**, No. 3, 253–257 (1995).